Optical–radio-frequency resonances free from power broadening

W. Chalupczak and P. Josephs-Franks
National Physical Laboratory, Hampton Road, Teddington, TW11 0LW, United Kingdom

S. Pustelny and W. Gawlik
Centrum Badań Magnetooptycznych, M. Smoluchowski Institute of Physics, Jagiellonian University, Reymonta 4, PL-30-059 Kraków, Poland

(Received 23 June 2009; revised manuscript received 30 October 2009; published 28 January 2010)

We have demonstrated a new mode of operation of an optical–radio-frequency double-resonance measurement, which allows high-resolution rf spectroscopy with negligible power broadening. The method is based on saturating, resonant excitation, and nonresonant detection of an atomic alignment of alkali-metal atoms by magneto-optical means. Its application to precision measurements, in particular to atomic magnetometry, is discussed.

DOI: 10.1103/PhysRevA.81.013422 PACS number(s): 32.60.+i, 42.65.−k

I. INTRODUCTION

The use of an optical–radio-frequency (rf) double-resonance technique has proved to be a powerful tool for various precision experiments ranging from the determination of hyperfine structure in excited states to single-atom interferometry [1,2]. The method originated in the 1950s and effectively aided the progress of high-resolution spectroscopy with noncoherent light sources [3]. The standard arrangement involves a resonant optical interaction that prepares an atomic sample placed in a static magnetic field. The interaction with the optical field causes a transfer of the polarization from the light beam to the atomic system, thereby creating an anisotropy in the distribution of internal states within the atomic medium. A static magnetic field gives rise to a separation of the Zeeman sublevels so that resonant transitions can be driven between them by an applied oscillatory magnetic field (rf frequency). Interaction with this rf field alters the anisotropy of the medium, which can be detected by changes in the resonance fluorescence or intensity or polarization modification of the light propagating through the sample.

The past decade has witnessed a revival of interest in the optical–rf double-resonance technique, which has been triggered by developments in the technology of atomic magnetometers, in particular in the rf domain [4–7]. The sensitivity of magnetometers has benefited from the long lifetime of the ground-state Zeeman sublevels pumped by an optical field. The relaxation rate of the ground-state observables (coherences and/or population anisotropies) is mainly determined by collisions of alkali-metal atoms with cell walls, a bulk metal surface, spin-exchange collisions with other atoms [8], and inhomogeneity of the magnetic field [9]. The collision rates scale linearly with atomic density, which might suggest using a low-density regime for reaching the highest sensitivity. However, the performance of the magnetometers also scales with the signal-to-noise ratio (SNR) and hence with atomic density. Several different configurations have thus been developed in an attempt to optimize the magnetic field measurement. In particular, a configuration of the magnetometer operating with a high density of alkali-metal atoms (10^{14} cm^{-3}) optically pumped by circularly polarized light allows a nearly complete elimination of the spin-exchange relaxation (linewidths about 400 Hz) [5]. While this kind of magnetometer has reached the highest sensitivity, a practical implementation of this mode of operation suffers from the complication of dealing with an atomic sample at a relatively high temperature (150°C). An alternative approach is to perform the measurements with atoms pumped by linearly polarized light into a so-called aligned state (sublevels with different values of $|M_F|$ being differently populated). An rf magnetometer in this configuration benefits from ultranarrow linewidths of the ground-state coherences (10 Hz), which are attainable with near-ambient-temperature atomic samples, but subsequently has a lower SNR [6,7].

In this article we present a new mode of operation of an optical–rf double-resonance technique, which employs detection based on the linear magneto-optical rotation and enables operation of the rf atomic magnetometer such that it combines the advantages of both of the methods described. In particular, it practically eliminates power broadening and yields an excellent SNR. The scheme relies on strong, saturating resonant excitation between $F = 4$ and $F' = 3$ hyperfine components of the cesium D_1 line (894 nm) [Fig. 1(a)] characterized by saturation parameter $G_{F=4} = \frac{\Omega^2}{\gamma\Gamma} = 10^4$, with the resonant Rabi frequency $\Omega = 100$ MHz, Γ (γ) being the excited-(ground-) state relaxation rate. This excitation pumps atoms into an aligned state in the $F = 4$ level but also transfers a fraction of the population to the "dark" $F = 3$ level and creates its alignment. The rf field applied perpendicularly to the magnetic field creates coherences and generates transitions between the ground-state Zeeman sublevels, in particular the $F = 3$ Zeeman sublevels. The rf transitions are monitored via rotation of the polarization plane of linearly polarized probe light. The difference in g factors of the $F = 3$ and $F = 4$ levels causes the rotation resonances to be detected at different rf frequencies. The $F = 3$ sublevels are then probed off-resonantly by the very same beam that is used for the optical pumping process. The small value of the off-resonant saturation parameter ($G_{F=3} = \frac{\Omega^2}{\gamma\Gamma+\Delta^2} = 10^{-4}$ for $\Delta = 9192.632$ MHz detuning) ensures a linear character of the probing; hence, it enables the observation of narrow rotation resonances, practically immune to power broadening.

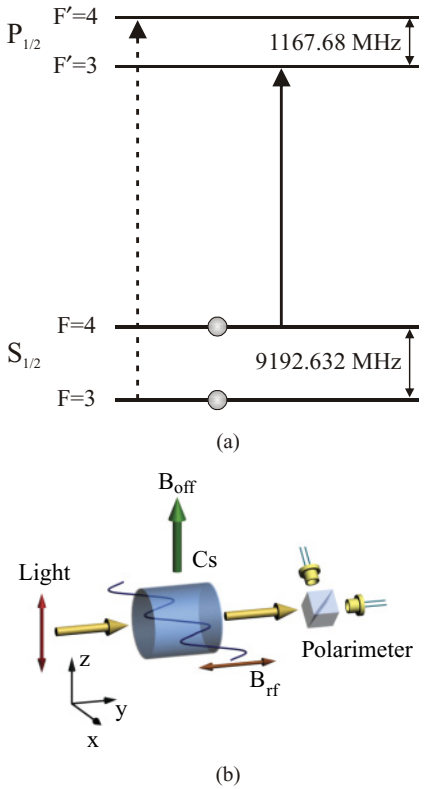

FIG. 1. (Color online) Energy structure of the cesium $6\,^2S_{1/2} \rightarrow 6\,^2P_{1/2}$ transition (D_1 line, 894 nm). The thick arrows (solid and dashed) represent the two frequencies of the laser beam used in the experiments. (b) Configuration of the double-resonance experiment involving linearly polarized light propagating along the y axis. The polarization of the laser beam is parallel to the direction of a static magnetic offset field $B_{\rm off}$ (z axis). The oscillating field $B_{\rm rf}$ is directed orthogonally to the static field.

II. EXPERIMENTAL SETUP

In our experiment a configuration similar to that of Ref. [6] is applied: a sample of thermal Cs atoms is placed in a static offset magnetic field aligned along the z axis ($B_{\rm off}$) and interacts with a single monochromatic laser beam propagating along y and linearly polarized in the z direction and an rf field oscillating in the y direction ($B_{\rm rf}$) [Fig. 1(b)]. With the quantization axis along z, the light beam has π polarization and drives the transitions between the ground and excited states with $M_{F'} - M_F = 0$. The atomic vapor is housed in an antirelaxation-coated cylindrical glass cell (diameter, 20 mm; length, 20 mm). Temperature-controlled water flowing through an oven (molded from CoolPoly polymer D5108 PPS; thermal conductivity, 10 W/mK) and in thermal contact with the vapor cell, allows the temperature of the vapor to be set. The ambient magnetic field is suppressed by use of five layers of cylindrical shields made from 2-mm-thick mu-metal with end caps. Additional rf shielding is provided by sheets of FerroxFoil on the innermost layer of the mu-metal shield. Measurements confirmed that the static shielding is better than 3×10^6. A set of two pairs of holes in the shields provides optical access along and orthogonal to the axis of the static magnetic field direction. The offset magnetic field, parallel to the polarization of the laser light, is created by an end-corrected solenoid (the residual relative field gradients over the length of the cell were measured to be less than 10^{-5}). Optical excitation is provided by a distributed-feedback laser operating at the D_1 line with 30 mW of output power. The frequency of the laser was locked to the $F = 4 \rightarrow F' = 3$ atomic transition using the Doppler-free dichroic lock technique [10] and additionally monitored with a standard saturation absorption setup. The amplitude of the laser beam was controlled by an acousto-optical modulator (AOM) set up in a double-pass configuration. The beam polarization was set by a zero-order wave plate and a Glan-Taylor polarizer (extinction better than 10^{-5}) and its diameter was 2 mm. An oscillating rf field is created by a set of coils orthogonal to the static offset field. The light transmitted through the cell is analyzed by a polarimeter consisting of a high-quality polarizing cube (extinction better then 10^{-5}) oriented at 45° with respect to the incident polarization and commercial balanced amplified photodetectors (Thorlabs, PDB 150). Implementation of the balanced polarimeter rather than detection of transmitted power helped to suppress technical laser-power noise. The two orthogonally polarized light beams at the cube outputs were recorded by two photodiodes and fed to a transimpedence amplifier, which generated an output voltage proportional to the difference between the photocurrents of the two photodiodes. The resulting signal was processed by either a lock-in amplifier or an rf spectrum analyzer.

III. RF RESONANCE SIGNALS

A. Magneto-optical rotation rf resonances for $F = 4$

A linearly polarized light beam creates alignment in the Zeeman sublevels of the $F = 4$ level as shown schematically in the inset to Fig. 2. An offset magnetic field, of the order of 143 μT, causes a splitting of the double-resonance signal via a nonlinear Zeeman effect, $2\nu_L^2/\nu_{\rm HFS} = 54$ Hz (ν_L being Larmor frequency, $\nu_{\rm HFS} = 9192.632$ MHz). Figure 2 represents the magneto-optical rotation signal recorded as the rf field is swept across the resonant frequencies of the transitions between the Zeeman sublevels of the ground-state hyperfine level $F = 4$ with 0.5 μW laser power. Since the

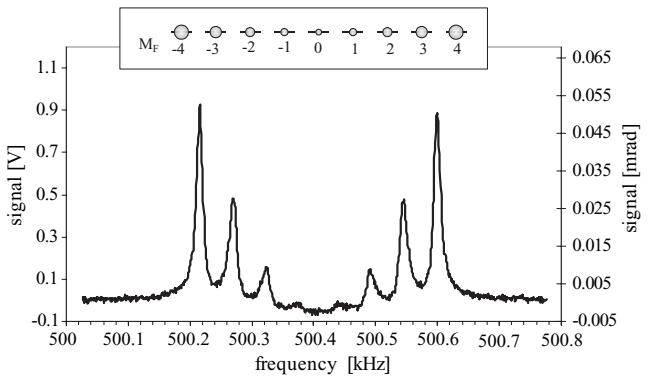

FIG. 2. Spectrum of the rf transition between nine Zeeman sublevels of the $F = 4$ ground level for an offset field of 143 μT. The frequency of the laser beam (0.5 μW power) was tuned to the $F = 4 \rightarrow F' = 3$ transition. The inset illustrates schematically the distribution of populations among the M_F sublevels (alignment), which yields the recorded signal.

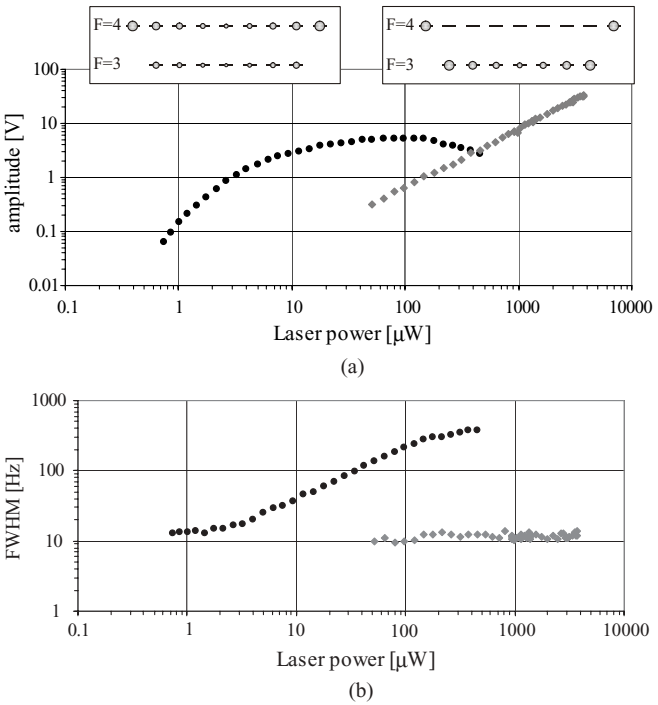

FIG. 3. Dependences of the signal amplitudes (a) and widths (b) of the double-resonance signals generated by atoms populating states $F = 4$ (black dots) and $F = 3$ (gray diamonds). The insets illustrate schematically the distributions of populations among the M_F sublevels (alignment), which yield the signals recorded in the two light-power regimes.

oscillatory field (B_{rf}) is applied orthogonally to the static field (B_{off}), it induces the $\Delta M_F = \pm 1$ transitions between the Zeeman sublevels. These transitions are revealed through the light beam's polarization rotation detected by the polarimeter. Consequently, there are eight features in Fig. 2 representing the rf transitions between sublevels with amplitudes determined by the relevant population differences, as well as Clebsch-Gordan coefficients and the laser detuning [11]. Thus, the amplitudes enable reconstruction of a population map of the M_F sublevels of the aligned state $F = 4$. The linewidth of the peaks is limited by spin-exchange relaxation, collisions of a gas atom with a bulk metal surface, or rf power broadening and is affected by optical power broadening for laser powers above 1 μW.

Black dots in Fig. 3(a) show the change of the signal amplitude and in Fig. 3(b) the change in the linewidth [full width at half maximum (FWHM)] of the dominant feature of the rf spectrum with increasing laser power. Intensity of the light recorded in each channel of the polarimeter depends on the incident light intensity I_0, angle of the polarization-plane rotation φ, and absorption of the medium characterized with the absorption coefficient κ $I_{\pm} = I_0 \sin^2(\frac{\pi}{4} \pm \varphi) \exp(-\kappa_{\pm} kL)$, where the $\pm$'s correspond to two circular components of linear polarization, k is the wave vector and L is the length of the sample [12]. For optically thin media and small rotations of the polarization plane, this can be rewritten into $I_{\pm} = I_0(1/2 \pm \varphi)$. In such cases, the quadratic dependence of the signal amplitude on the laser power, seen below $\sim 2.5\,\mu$W, confirms the nonlinear character of the signal. Estimation of the resonant saturation parameter, $G_{F=4}$, based on the power broadening

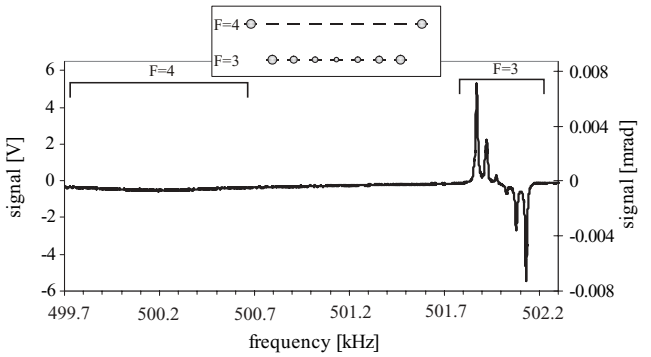

FIG. 4. The rf spectrum of the transitions among the Zeeman sublevels of the states $F = 4$ (small, broad feature around 500.2 kHz) and $F = 3$ (six narrow features around 502 kHz). The frequency of the laser beam (2 mW power) was tuned to the $F = 4 \rightarrow F' = 3$ transition. The signal generated by the $F = 4$ atoms is reduced by the strong saturation and power broadening. The inset illustrates schematically the population distributions in the $F = 3$ and $F = 4$ levels.

of the linewidth (about 0.4 kHz for 0.5 mW), gives a value of the order of 10^4. Strong saturation causes a nearly complete depletion of the $|M_F| \leqslant 3$ components of the $F = 4$ state. Their population is transferred to the $M_F = \pm 4$ components of $F = 4$ and to the $F = 3$ level via optical pumping. These population redistributions corresponding to weak and intense light regimes are shown schematically in insets to Fig. 3. It is the optical pumping of the $F = 3$ level that is responsible for the signals described below.

B. Power-broadening-free $F = 3$ resonances

For low laser power, only the resonances which are associated with the directly pumped state are observed, that is, with $F = 4$ for the laser resonant with the $F = 4 \rightarrow F' = 3$ transition (Fig. 2). However, for higher laser power, the magneto-optical rotation signal reveals resonances associated with the alignment of the $F = 3$ hyperfine ground state, while the $F = 4$ signal is barely visible because of the strong saturation and power broadening. Figure 4 shows a typical magneto-optical rotation signal observed during an rf field sweep for a laser power of 2 mW. Due to the difference in the Lande factors between two hyperfine components of cesium ($g_F = 0.250390$ for $F = 4$ and $g_F = -0.251194$ for $F = 3$ [13]), these resonances are shifted by 1.5 kHz with respect to the $F = 4$ resonances at a field of 143 μT [14]. At that light power, the signal from the $F = 3$ level is visible with a very high SNR as the group of six narrow, resolved lines (about 10 Hz). In the same way as in the case of $F = 4$ (Fig. 2), their amplitudes reflect the population distributions of the M_F sublevels while their signs result from the detuning of the laser and signs of Clebsch-Gordan coefficients [11].

The alignment in the $F = 3$ ground hyperfine level results from the transfer of the alignment of the $F = 4$ atoms by the optical pumping process. The linear dependence of the signal amplitude on laser power, depicted by gray diamonds in Fig. 3(a), points to the spontaneous emission mechanism in the preparation of the $F = 3$ alignment and to the complete population transfer of the $|M_{\mathrm{F}}| \leqslant 3$ sublevels of $F = 4$ to

$F=3$. Since the frequency of the beam, which probes the $F=4 \rightarrow F'=3$ transition, is detuned by 9192.632 MHz from the $F=3 \rightarrow F'=3$ transition, the effect of optical power broadening on the $F=3$ resonances is negligible (nonresonant saturation parameter, $G_{F=3}=10^{-4}$). No change in the linewidth of the resonance lines is observed with laser powers from 50 μW to 4 mW for ambient-temperature atoms [Fig. 3(b), gray diamonds], which confirms the "dark-state" character of that state. At the same time, huge power broadening largely exceeds the separation between the individual rf resonances in the $F=4$ state and makes them completely invisible. When the temperature rises to 32.5°C, the spin-exchange relaxation limited linewidth increases to 30 Hz and its dependence on the laser power is consistent with the above value of the saturation parameter.

We have also measured the dependence of the linewidths of the $F=3$ resonances on the rf power. An estimation of the rf saturation parameter at which the data were taken gives a value of the order of 0.6 and extrapolation of the linewidth to zero rf power yielded 8 Hz, which is consistent with the value presented in Ref. [15].

To confirm the above-outlined mechanism of the spontaneous alignment transfer, the laser was tuned to the $F=3 \rightarrow F'=4$ transition [broken line in Fig. 1(a)] and the double-resonance signal contributions from the $F=4$ and $F=3$ were recorded again. Figure 5 presents such signal recorded for a laser power of 2 mW. This time, with the strong laser beam pumping at the $F=3 \rightarrow F'=4$ transition, all M_F sublevels of the $F=3$ state are depleted and, consequently, the amplitude of the $F=3$ contribution is completely negligible. We have also observed optical pumping between the $F=4$ and $F=3$ levels with excitation on the $F=4 \rightarrow F'=4$ transition that built up the population of the $M_F=0$ sublevel (not shown).

It was pointed out in [11] that the sign of the double-resonance signal depended not only on the population differences between the sublevels but also on the probe laser detuning (the detuning of the pump laser contributed solely to the value of the population difference). Although the calculations and observations in [11] were done with reference to hyperfine structure, our measurements confirmed that the analogous model holds also for Zeeman sublevels. While

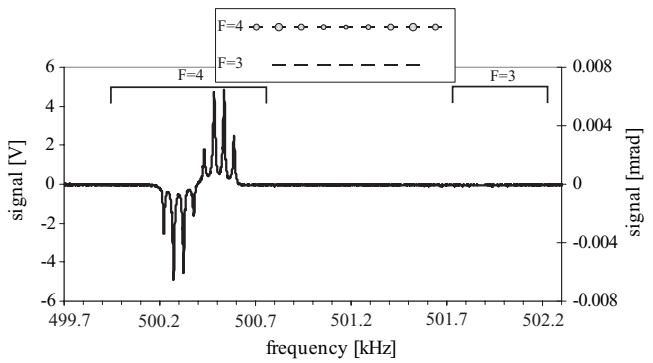

FIG. 5. The rf spectrum of the transitions among the Zeeman sublevels of $F=4$. The frequency of the laser beam (2 mW power) was tuned to the $F=3 \rightarrow F'=4$ transition. The inset shows schematically the related population distributions, alignment in $F=4$, and the total depletion of $F=3$.

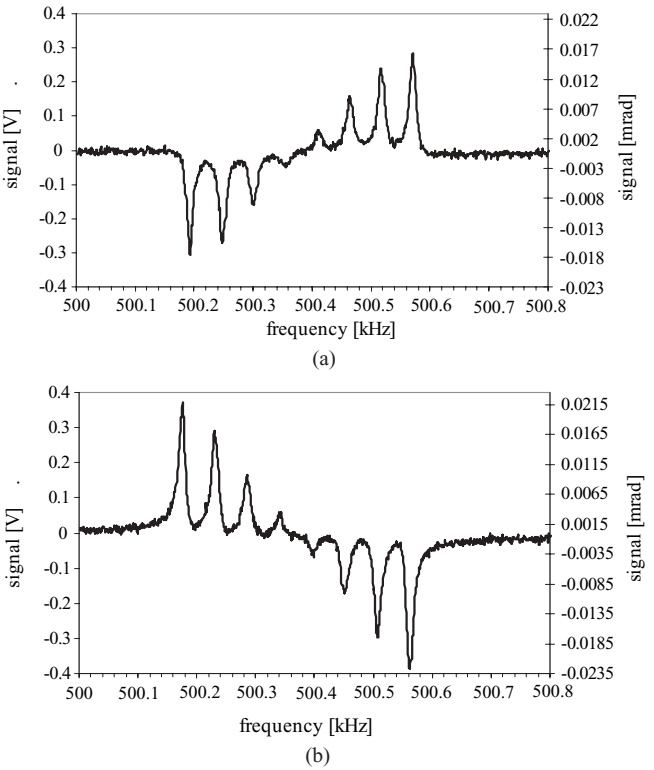

FIG. 6. Spectrum of the rf transition between nine Zeeman sublevels of the $F=4$ ground level for an offset field of 143 μT. The laser beam (0.5 μW power) was tuned +360 MHz (a) or –360 MHz (b) away from the frequency of the $F=4 \rightarrow F'=3$ transition.

most of our experiments were done with the laser tuned to the resonance of the $F=4 \rightarrow F'=3$ transition (see rf spectrum in Fig. 2), we also observed rf spectra for laser tuned $\pm$360 MHz away from the resonance (by choosing the appropriate diffraction order at an AOM in the locking system or main beam). Figures 6(a) and 6(b) represent two rf spectra taken with opposite detunings of the laser from the resonant transition recorded under the same conditions as Fig. 2. Since the laser detuning largely exceeds the 500 kHz Zeeman splitting, the relative signs between different Zeeman components depend only on population differences, while the change of sign between spectra in Figs. 6(a) and 6(b) corresponds to the opposite signs of the laser detunings. Another consequence of the $\pm$360 MHz laser detuning is that the amplitudes of the resonance features in Fig. 6 are smaller than those in Fig. 2. A more detailed analysis of this effect goes beyond the scope of this article and will be published elsewhere.

IV. RF MAGNETOMETER PERFORMANCE

In the following part we concentrate on discussing the essential differences in performance of the rf magnetometers based on alignment configuration in the standard and in the novel power-broadening-free modes rather than optimization of absolute sensitivity. As mentioned before, power-broadening-free $F=3$ resonances were observed for a wide range of the offset magnetic fields (0.286–143 μT). For magnetic fields above 72 μT, the optical–rf double-resonance

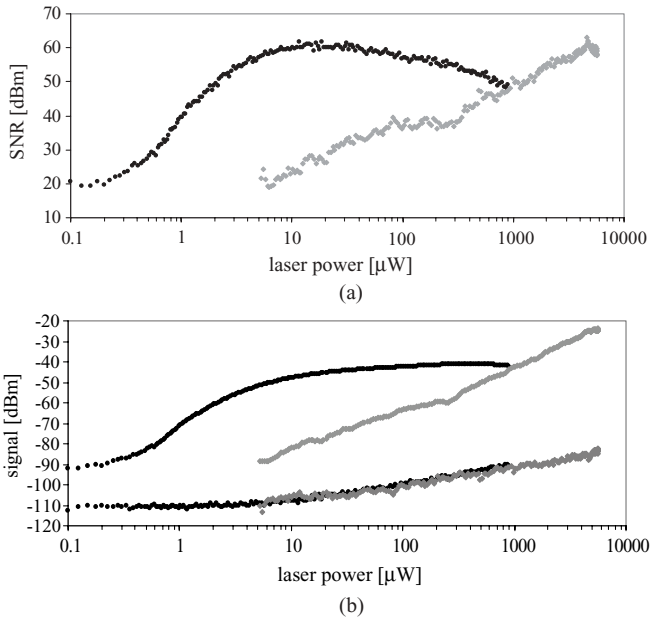

FIG. 7. Dependence of SNR (a) and the signal amplitude, background (rf turned off) (b) measured by the rf spectrum analyzer (10 Hz bandwidth) as a function of laser power for standard (atoms in $F = 4$; black dots) and power-broadening-free (atoms in $F = 3$, gray diamonds) configurations. The flat part of the background signal (a) represents the detection noise (commercial system of balanced photodiodes) while for laser powers above 20 μW optical noise becomes the leading contribution. For the standard configuration, the optimum of the SNR appears for 20 μW, while in power-broadening-free mode the SNR increases over whole range of laser powers (b). The offset magnetic field is 143 μT, while the temperature of the sample is equal to 18°C.

signals are deteriorated by the nonlinear Zeeman effect. Recently, however, it was demonstrated that this adverse effect could be largely compensated by light shifts [16].

In order to demonstrate the differences in performance of the rf magnetometers operating in the two discussed modes, we examined the dependence of the SNR on the laser power. The frequency of the rf field was tuned to one of the maxima of the relevant rf spectrum (Figs. 2 and 4) and the amplitude of the signal at the rf spectrum analyzer was monitored. Figure 7 shows the dependence of SNR [Fig. 7(a)] and the signal amplitude (rf on) compared with the background (rf off) [Fig. 7(b)] on laser power for both. For the standard configuration the optimum of the SNR appears at around 20 μW followed by a decrease due to saturation, while in the power-broadening-free mode the SNR increases over the whole range of the laser powers. Some irregularities in the approximately linear increase of the $F = 3$ signal might be caused by a drift of the rf generator or the offset field [16]. The flat part of the background signal (rf field switched off and laser power below 3 μW) represents the detection noise, while for higher laser powers optical shot noise becomes the leading contribution. In particular, Fig. 7(b) confirms that the electronic (detection) noise is significant for laser powers in the range around 20 μW (optimum SNR). It also shows that the noise level for signal from atoms in $F = 3$ is fully defined by optical noise. In order to evaluate the sensitivities of the

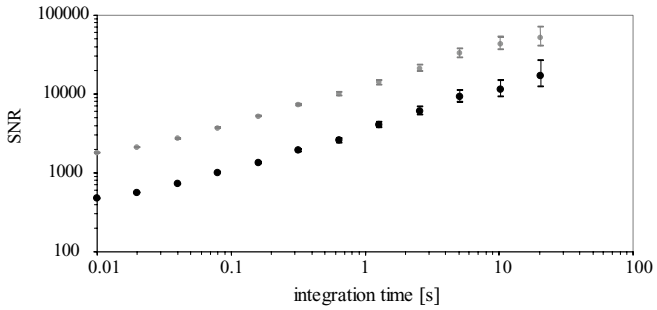

FIG. 8. Allan deviation of the SNR for the signal generated by atoms in $F = 3$ limited by the optical (black circles) and the detection noise (gray circles) (laser power, 5.5 mW; offset magnetic field, 143 μT; temperature of sample, 30°C).

rf magnetometer operating in the two modes, we have used Allan deviation, which is an alternative approach to standard Fourier analysis. Allan deviation not only helps to specify noise characteristics (white, flicker) but also demonstrates system performance on longer time scales. With an rf probe field of 10 nT, the rf noise at 1 s was observed at the 10^{-4} level limited by the laser shot noise for the power-broadening-free method (Fig. 8) and by the detection noise for the standard configuration. The absence of long-term drifts in the noise levels and constant $\sqrt{t}$ value of the slope demonstrate the white character of the noise. As demonstrated in Fig. 7(a), for the power-broadening-free mode the saturation of the SNR has not been reached and hence the results could be further improved by implementation of more powerful lasers. Another improvement might be optimization of cell temperature or atomic density.

V. SUMMARY AND CONCLUSIONS

Recent developments in the technology of atomic magnetometers have demonstrated sensitivities in the fT range and created a vast field of new applications, ranging from health-sector systems of magnetic resonance imaging [17] and magnetoencephalography [18] to defense and security technology of nuclear quadrupole resonance [19]. The most sensitive devices operate with a potassium sample at 190°C and require high-power lasers [19]. On the other hand, the off-resonance mode of operation of the optical–rf double resonance presented earlier in this article is characterized by a high SNR along with signal linewidths unperturbed by the optical field, even with high laser powers. This results from strong resonant optical pumping which saturates the resonant transition and creates, via spontaneous emission, alignment in the otherwise noninteracting (dark) state. With laser light tuned to the $F = 4 \rightarrow F' = 3$ transition and appropriately high optical power (0.1- to 1-mW range), nearly all of the population of the initial sublevels is removed to the external $M_F = \pm 4$ sublevels of the $F = 4$ which cannot be coupled by light and to the Zeeman sublevels of the $F = 3$. The laser light is far detuned from the latter state and hence the state can only be probed nonresonantly. The nonresonant character of the interaction is responsible for the very low saturation ($G_{F=3} = 10^{-4}$) and gives rise to the lack of power broadening of the corresponding magneto-optical resonances. For such

a low saturation parameter, the interaction with the state is linear, which explains the linear dependence of the resonances' amplitudes on light intensity (Fig. 3).

The power-broadening-free mode benefits from simplicity of instrumentation and operation at ambient temperature and a possibility of achieving high-sensitivity of magnetic-field measurements. In a standard measurement, based on atomic alignment, the optimum performance is usually obtained using laser powers of several μW. With such small powers the electronic noise of the detection system becomes significant. The minimum noise-equivalent power of the commercial detector we used was 7 pW/Hz$^{1/2}$, which is equivalent to the shot noise of a 14-μW laser beam. The ability to operate the magnetometer at higher laser powers without compromising the sensitivity (thanks to the lack of power broadening) removes the detection noise as a limiting factor in the device's performance. The easy access to the signal generated by atoms populating the $F = 4$ as well as the $F = 3$ state provides an opportunity to verify the efficiency of the sample polarization, which becomes important in ultrasensitive rf magnetometry [20] and quantum-information processing applications.

The power-broadening-free mode is fundamentally similar to the coherent population trapping (CPT) dc magnetometers, where the position of narrow Zeeman-shifted CPT resonances is measured [21]. In CPT devices the interaction with a strong (pump) field produces the nonabsorbing state probed by a weak probe field. In both cases, atoms (in the $F = 3$ state in our case or dark state in the CPT method) are decoupled from the pump beam while being probed. A CPT magnetometer requires two different fields, whereas in our case the same field acts as both the pump and the probe.

ACKNOWLEDGMENTS

The NPL authors acknowledge discussions with Professor T. Dohnalik and Dr. R. Godun and support from the UK Ministry of Defence (Competition of Ideas project A638). The UJ authors thank the Polish Ministry of Science and Higher Education (Grant Nos. NN 505 0920 33 and NN 202 0741 35). Part of the work was supported by the European Union within the Innovative Economy Framework Program "Team Project" operated by the Foundation for Polish Science.

[1] J. Brossel and F. Bitter, Phys. Rev. **86**, 308 (1952).

[2] R. Huesmann, Ch. Balzer, Ph. Courteille, W. Neuhauser, and P. E. Toschek, Phys. Rev. Lett. **82**, 1611 (1999).

[3] G. J. Ritter and G. W. Series, Proc. R. Soc. London A **238**, 473 (1957).

[4] E. B. Aleksandrov and M. V. Balabas, Opt. Spektrosk. **69**, 8 (1990); S. Groeger, G. Bison, J. L. Schenker, R. Wynands, and A. Weis, Eur. Phys. J. D **38**, 239 (2006).

[5] I. M. Savukov, S. J. Seltzer, M. V. Romalis, and K. L. Sauer, Phys. Rev. Lett. **95**, 063004 (2005); M. P. Ledbetter, I. M. Savukov, V. M. Acosta, D. Budker, and M. V. Romalis, Phys. Rev. A **77**, 033408 (2008).

[6] M. P. Ledbetter, V. M. Acosta, S. M. Rochester, D. Budker, S. Pustelny, and V. V. Yashchuk, Phys. Rev. A **75**, 023405 (2007).

[7] A. Weis, G. Bison, and A. S. Pazgalev, Phys. Rev. A **74**, 033401 (2006); G. Di Domenico, G. Bison, S. Groeger, P. Knowles, A. S. Pazgalev, M. Rebetez, H. Saudan, and A. Weis, *ibid.* **74**, 063415 (2006); G. Di Domenico, H. Saudan, G. Bison, P. Knowles, and A. Weis, *ibid.* **76**, 023407 (2007).

[8] D. Budker, L. Hollberg, D. F. Kimball, J. Kitching, S. Pustelny, and V. V. Yashchuk, Phys. Rev. A **71**, 012903 (2005).

[9] S. Pustelny, D. F. Jackson Kimball, S. M. Rochester, V. V. Yashchuk, and D. Budker, Phys. Rev. A **74**, 063406 (2006).

[10] G. Wasik, W. Gawlik, J. Zachorowski, and W. Zawadzki, Appl. Phys. B **75**, 613 (2002).

[11] J. Skalla, S. Lang, and G. Wäckerle, J. Opt. Soc. Am. B **12**, 772 (1995).

[12] S. Pustelny, W. Lewoczko, and W. Gawlik, J. Opt. Soc. Am. B **22**, 37 (2005).

[13] N. F. Ramsey, *Molecular Beams* (Oxford University Press, London, 1956).

[14] Assuming the resonance linewidth of 10 Hz, one arrives at about 1 μT of a minimal magnetic offset field that allows, in principle, observation of splitting of the $F = 4$ and $F = 3$ resonances. A trace of the $F = 3$ resonance was indeed observed in [7] in a 2.83 μT (9.9 kHz) field. However, as evident from Fig. 3(a), observation of the $F = 3$ signal for weak rf fields (about 1 nT) requires laser powers on the order of 100 μW or higher. In other words, signals generated by atoms in the $F = 4$ and $F = 3$ states appear in different laser power regimes. We have observed signals from those two groups of the atoms for the offset magnetic field as low as 0.286 μT.

[15] B. Julsgaard, J. Sherson, J. L. Sorensen, and E. S. Polzik, J. Opt. B: Quantum Semiclass. Opt. **6**, 5 (2004).

[16] K. Jensen, V. M. Acosta, J. M. Higbie, M. P. Ledbetter, S. M. Rochester, and D. Budker, Phys. Rev. A **79**, 023406 (2009).

[17] I. M. Savukov and M. V. Romalis, Phys. Rev. Lett. **94**, 123001 (2005).

[18] H. Xia, A. Ben-Amar Baranga, D. Hoffman, and M. V. Romalis, Appl. Phys. Lett. **89**, 211104 (2006).

[19] S. K. Lee, K. L. Sauer, S. J. Seltzer, O. Alem, and M. V. Romalis, Appl. Phys. Lett. **89**, 214106 (2006).

[20] W. Wasilewski, K. Jensen, H. Krauter, J. J. Renema, M. V. Balabas, and E. S. Polzik, e-print arXiv:0907.2453.

[21] M. Fleischhauer and M. O. Scully, Phys. Rev. Lett. **69**, 1360 (1992); M. O. Scully and M. Fleischhauer, Phys. Rev. A **49**, 1973 (1994); A. Nagel, L. Graf, A. Naumov, E. Mariotti, V. Biancalana, D. Meschede, and R. Wynands, Europhys. Lett. **44**, 31 (1998); L. Guo-Bin, D. Run-Chang, L. Chao-Yang, and G. Si Hong, Chin. Phys. Lett. **25**, 472 (2008); J. Belfi, G. Bevilacqua, V. Biancalana, Y. Dancheva, and L. Moi, J. Opt. Soc. Am. B **24**, 1482 (2007), and references therein.